Front. Mater. Sci. 2025, 19(2): 250731
https://doi.org/10.1007/s11706-025-0731-2

RESEARCH ARTICLE

Facile synthesis of Ru-incorporated NiFe–MOF nanosheet heterostructures as an efficient bifunctional electrocatalyst

Fangqing Zou[1,2], Ye Xiao[2], Xianshu Qiao[1], Chuanjin Tian (✉)[1], and Chang-An Wang (✉)[2]

1 Jiangxi Key Laboratory of Advanced Ceramic Materials, School of Materials Science and Engineering, Jingdezhen Ceramic University, Jingdezhen 333403, China
2 State Key Laboratory of New Ceramic Materials, School of Materials Science and Engineering, Tsinghua University, Beijing 100084, China

ABSTRACT: Constructing specific noble metal/metal–organic framework (MOF) nano-heterostructures is an effective strategy for promoting water electrolysis, yet remains highly challenging due to complex synthesis methods, difficulties in structural characterization, and the demanding nature of performance optimization. In this work, a heterojunction electrocatalyst was developed through growing Ru nanoparticles on NiFe–MOF nanosheets (NSs) supported by nickel foam (NF) using an easily accessible solvothermal method followed by an annealing strategy. Owing to the electronic interaction between Ru nanoparticles and NiFe–MOF NSs, the optimized Ru@NiFe–MOF/NF catalyst exhibits excellent bifunctional performance for the hydrogen evolution reaction (with an overpotential of 84 mV at 10 mA·cm^{-2}) and the oxygen evolution reaction (with an overpotential of 240 mV at 10 mA·cm^{-2}) in a 1.0 mol·L^{-1} KOH solution, which is superior to that of commercial catalysts. This study highlights a promising strategy for designing and developing efficient electrocatalysts for overall water electrolysis.

KEYWORDS: Ru@NiFe–MOF/NF; catalytic performance; oxygen evolution reaction; hydrogen evolution reaction; nanosheet; heterostructure

Contents

Received April 3, 2025; accepted April 24, 2025

E-mails: tiancj11@139.com (C.T.), wangca@mail.tsinghua.edu.cn (C.W.)

1 Introduction

The increasing consumption of fossil fuels and the worsening living environment have driven the exploration of environmentally friendly and sustainable energy sources as alternatives to traditional fossil fuels [1]. Hydrogen energy has attracted great attention from

researchers due to its high energy density and environmental friendliness [2]. Hydrogen is regarded as the most promising substitute, and hydrogen production by water electrolysis is an important means to achieve industrialized and low-cost hydrogen generation [3–4]. However, its sluggish reaction kinetics need to be overcome by means of effective electrocatalysts [5–6]. Water electrolysis involves two half-reactions, namely hydrogen evolution reaction (HER) and oxygen evolution reaction (OER). As for such two reactions, OER involves multi-electron transfer steps and has a relatively higher energy barrier, which greatly hinders the large-scale hydrogen production on an industrial scale [7–9]. Currently, noble metal-based catalysts, such as Pt/C and IrO_2/RuO_2, can achieve high electrocatalytic efficiencies and are the benchmark catalysts for HER and OER, respectively [10]. However, the high cost and scarcity have hindered their widespread application and driven people to seek cheaper and more efficient electrocatalysts [11–14]. In addition, most of these catalysts are powdered materials and usually need to be combined with a polymer binder (Nafion) before loading onto the electrodes, which inevitably increases the electrode interface impedance and reduces the catalytic activity [15]. Powdered catalysts are also prone to detachment from the electrode surface during the gas evolution, thereby significantly reducing the cycling stability of catalysts [16–19]. Therefore, it is of vital importance to design and develop self-supported catalysts with a low noble metal content for HER and OER.

In recent years, a great number of first-row transition metal alloy catalysts have been widely studied due to their abundant terrestrial resources, low cost and excellent electrocatalytic activity, such as Fe_2Ni [20], NiZn [21], NiCo [22], and ZnNiCo [23] alloys. Metal–organic frameworks (MOFs), a novel class of porous crystalline materials [24–25], are composed of a variety of organic ligands and metal centers, with a wide range of applications such as water electrolysis [26], gas storage [27], and metal–air batteries [28]. Due to the flexible tunability and well-defined structure of MOFs, they have become promising models for the design of catalysts at the molecular level. However, when directly used as electrocatalysts for OER and HER, pristine MOFs usually only exhibit single catalytic activity and inefficient electrochemical performance, thus failing to achieve the expected result. Researchers have made numerous attempts to improve the catalytic efficiency of MOFs. One of the most effective methods is to integrate a small amount of noble metals (Ru or Ir) with high electrocatalytic activity into MOF precursors that have the advantage of low cost. For instance, Sun et al. introduced single-atom dispersed Ru into Ni–benzene dicarboxylic acid (BDC), and the synthesized catalyst exhibited excellent catalytic activity for HER under all pH values [1]. Li et al. used Ru-modified CoNi–1,3,5-benzenetricarboxylic acid (BTC) for the preparation of catalysts, achieving the outstanding electrocatalytic performance in both KOH and seawater environments [2]. A multimetallic MOF-derived high-entropy alloy (HEA) catalyst, CC@FeCoNiMoRu-HEA/C, designed by Hu et al. has excellent OER catalytic activity and strong durability while reducing the content of Ru and lowering the economic cost [12].

In this study, Ru-modified NiFe–MOF nanosheets (NSs) were synthesized on nickel foam (NF) through a one-step hydrothermal method via spontaneous reduction–oxidation (redox) reactions and coordination reactions. The Ru@NiFe–MOF/NF catalyst was subsequently prepared via the annealing treatment. The introduction of NiFe–MOFs promoted the dispersion of Ru throughout the framework, providing the possibility of the improvement in the electrocatalytic performance of bifunctional Ru-based catalysts. Experimental studies show that the introduction of Ru atoms has changed the electronic structure of Ni atoms through metal–ligand interactions, thereby enhancing the intrinsic electrocatalytic activity and enhancing the electrocatalytic performance of Ru@NiFe–MOF/NF for HER and OER. In addition, Ru@NiFe–MOF/NF also has great potential for hydrogen production via water electrolysis in an alkaline environment due to its excellent activity and stability. The excellent electrocatalytic activity of Ru@NiFe–MOF/NF was thoroughly investigated through various experiments and structural characterizations. The design and synthesis of Ru@NiFe–MOF/NF provide new insights and research directions, paving the way for continuous hydrogen production in practical situations.

2 Experimental

2.1 Materials

NF (1 mm in thickness) was purchased from Suzhou Shuerte Industrial Technology Co., Ltd. Ruthenium

chloride hydrate ($RuCl_3 \cdot xH_2O$, guaranteed reagent (GR)) was obtained from Sinopharm Chemical Reagent Co., Ltd. Hydrochloric acid (HCl, 36 wt.%) was sourced from Beijing Beihua Fine Chemicals Co., Ltd. Potassium hydroxide (KOH, 85%) was acquired from Aladdin Co., Ltd. Nickel nitrate hexahydrate ($Ni(NO_3)_2 \cdot 6H_2O$, analytical reagent (AR)) was purchased from Sinopharm Chemical Reagent Co., Ltd. Iron(III) nitrate nonahydrate ($Fe(NO_3)_3 \cdot 9H_2O$, AR) was supplied by Xilong Scientific Co., Ltd. Cobalt nitrate hexahydrate ($Co(NO_3)_2 \cdot 6H_2O$, AR) was acquired from Shanghai Zhanyun Chemical Co., Ltd. Terephthalic acid (PTA, purity 99%) was obtained from Aladdin Co., Ltd. Absolute ethanol (ethanol absolute, density of 0.7893 $g \cdot mL^{-1}$) was sourced from Tianjin Yufutai Chemical Reagent Co., Ltd. N,N-dimethylformamide (DMF, AR). The commercial 20 wt.% Pt/C catalyst was procured from Shanghai Hesen Electric Co., Ltd. The commercial RuO_2 catalyst (purity 99.95%) was purchased from Alfa Aesar Co., Ltd. The Nafion solution (5 wt.%) was acquired from InnoChem Co., Ltd. Deionized water (DIW) used throughout the entire experiment was self-made in the laboratory, and all chemicals and solvents were not subjected to further purification.

2.2 Preparation of catalysts

First, NF was cut into small pieces followed by ultrasonic cleaning with 3 $mol \cdot L^{-1}$ HCl for 15 min to remove surface oxides and organic contaminants. Then they were rinsed with DIW and dried. Next, a homogeneous solution was prepared, which included ethanol (1.5 mL), DIW (1.5 mL), PTA (80 mg), DMF (30 mL), and $Ni(NO_3)_2 \cdot 6H_2O$ (0.140 g). Subsequently, the cleaned NF was immersed in this solution and transferred to a 100 mL polytetrafluoroethylene (PTFE)-lined autoclave. After maintaining at 125 °C for 12 h to allow the growth of MOFs on the NF substrate, the resulting product was rinsed with DIW and dried at 50 °C for 8 h. Ni–MOF/NF was finally obtained after annealing at 350 °C for 3 h under an argon atmosphere.

For the preparation of NiFe–MOF/NF, 0.164 g $Fe(NO_3)_3 \cdot 9H_2O$ was added. For Ru@Ni–MOF/NF, 0.003 g $RuCl_3 \cdot xH_2O$ was added. For Ru@Fe–MOF/NF, $Ni(NO_3)_2 \cdot 6H_2O$ was replaced with 0.164 g $Fe(NO_3)_3 \cdot 9H_2O$ based on the preparation procedure of Ru@Ni–MOF/NF. For Ru@NiFe–MOF/NF, 0.164 g $Fe(NO_3)_3 \cdot 9H_2O$ was additionally incorporated into the synthesis of Ru@Ni–MOF/NF. For Ru@NiCo–MOF/NF, 0.118 g $Co(NO_3)_2 \cdot 6H_2O$ was additionally added in the preparation of Ru@Ni–MOF/NF. All other experimental conditions remain the same.

3 Results and discussion

The synthesis process of Ru@NiFe–MOF/NF is illustrated in Scheme 1. In this process, NF not only serves as a conductive substrate supporting the catalyst, but also acts as a reducing agent to effectively reduce Ru^{3+} ions to metallic Ru due to the favorable chemical process ($\Delta E = E(Ru^{3+}/Ru) - E(Ni^{2+}/Ni) > 0$, where $E(Ni^{2+}/Ni) = -0.257$ V and $E(Ru^{3+}/Ru) = +0.704$ V) [29]. Meanwhile, using $Ni(NO_3)_2 \cdot 6H_2O$ and $Fe(NO_3)_3 \cdot 9H_2O$ as metal sources and PTA as a ligand, ultrathin NiFe–MOF NS arrays were grown on NF. Benefiting from the two simultaneous reaction processes, Ru nanoparticles (NPs) were embedded into NiFe–MOFs, followed by *in-situ* self-assembling and growth on the surface of NF, and the resulting product is hereafter denoted as Ru@NiFe–MOF/NF.

Figure 1(a) shows the scanning electron microscopy (SEM) image of three-dimensional (3D) NiFe–MOF NSs with smooth surfaces assembled on NF. The micron-scale spherical aggregates on the NF are NiFe–MOFs, which

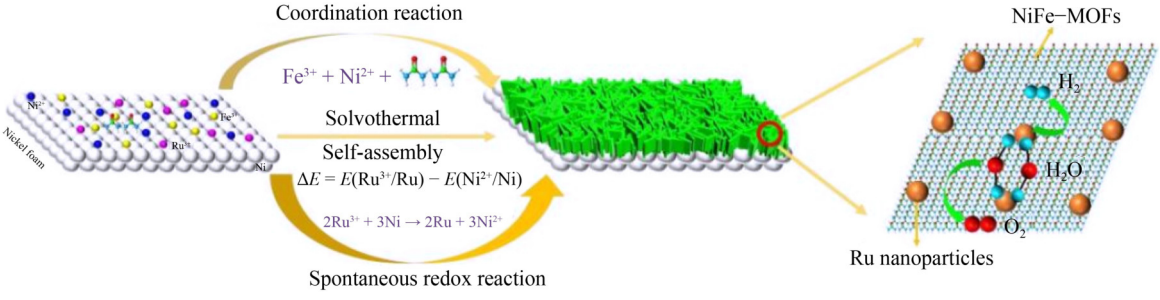

Scheme 1 Schematic illustration of the synthesis of Ru@NiFe–MOF/NF.

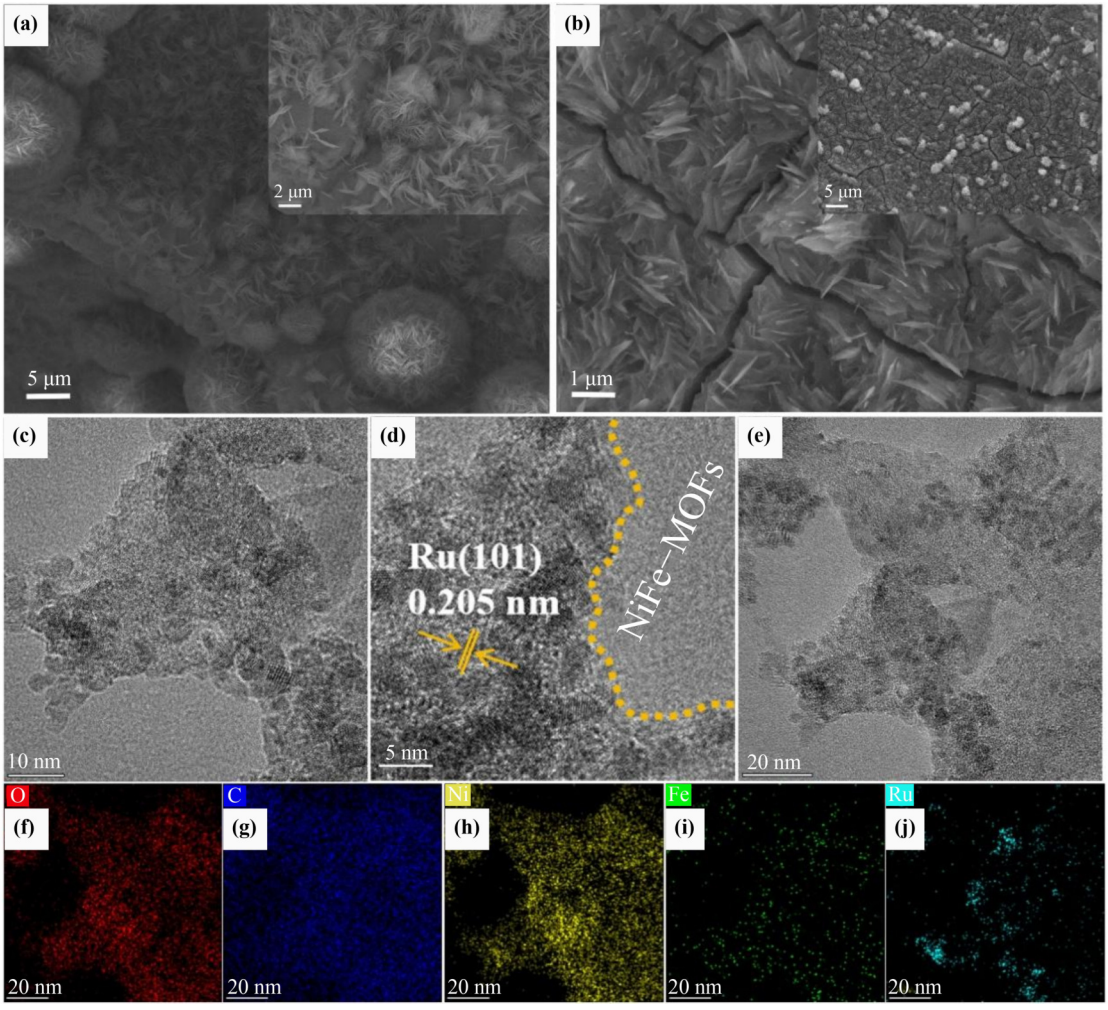

Fig. 1 (**a**)(**b**) SEM images of NiFe–MOF/NF (left panel) and Ru@NiFe–MOF/NF (right panel). (**c**) TEM image of Ru@NiFe–MOF/NF. (**d**) HRTEM image of Ru@NiFe–MOF/NF. (**e**)(**f**)(**g**)(**h**)(**i**)(**j**) HAADF-STEM image and related elemental mappings of Ru@NiFe–MOF/NF.

exhibit an interconnected network that facilitates electrolyte penetration and, in particularly, enables more Ru active sites to be exposed. Surprisingly, upon the incorporation of Ru^{3+}, the original smooth NiFe–MOF NSs develop surface roughening, as evidenced in Fig. 1(b) along with Fig. S1 (included by ESM of Appendix). This structural evolution suggests the critical role of Ru NPs in modulating the morphology of MOFs. As shown in Fig. S2 (included by ESM of Appendix), disordered ultrathin Ni–MOF NS arrays grew on Ru@Ni–MOF/NF, maintaining their structural integrity without detectable surface roughening upon the incorporation of Ru^{3+}. Fe–MOFs did not exist in the form of ultrathin NS arrays on NF, but as particles rich in defects, as shown in Fig. S3 (included by ESM of Appendix). Notably, NiCo–MOFs exhibit symmetrical flowers on both sides. It was precisely this unique structure that provided abundant attachment sites for Ru^{3+}. However, the insufficient interparticle connectivity within NiCo–MOFs impedes charge/mass transport dynamics, thereby adversely affecting the OER/HER kinetics to some extent, as shown in Fig. S4 (included by ESM of Appendix).

In addition, transmission electron microscopy (TEM) images of Ru@NiFe–MOF/NF show the uniform distribution of Ru NPs with an average diameter of approximately 4 nm in Fig. 1(c) along with Fig. S5 (included by ESM of Appendix). The high-resolution transmission electron microscopy (HRTEM) image of Ru@NiFe–MOF/NF in Fig. 1(d) shows lattice fringes of the Ru (1 0 0) plane with a lattice spacing of 0.205 nm. Importantly, the strong interfacial interaction between Ru NPs and NiFe–MOFs is evident from the clear interfacial structure observed. As reported in previous works, the performance of heterogeneous catalysis is strongly

influenced by the surface and interface properties, because the interface structure can modify the active sites to adjust the bonding strength of reaction intermediates, thereby improving the sluggish water electrolysis reaction. Furthermore, the selected-area electron diffraction (SAED) pattern shown in Fig. S6 (included by ESM of Appendix) indicates that Ru@NiFe–MOF/NF exhibits a polycrystalline structure with the (1 1 1) plane of NiO, the (1 0 1) plane of Ru, and the (2 0 0) plane of Ni.

The existence of the element Ru was further confirmed by the analyses on high-angle annular dark-field scanning transmission electron microscopy (HAADF-STEM) and energy-dispersive X-ray spectroscopy (EDS) images of Ru@NiFe–MOF/NF in Figs. 1(e)–1(j), indicating that the elements Ni, Fe, Ru, C and O were uniformly distributed (Fig. S7 (included by ESM of Appendix)). Based on the EDS analysis, the elemental contents of C, O, Fe, Ni, and Ru in the Ru@NiFe–MOF/NF catalyst are summarized in Table S1 (included by ESM of Appendix).

X-ray diffraction (XRD) patterns of Ru@Ni–MOF/NF, Ru@Fe–MOF/NF, Ru@NiFe–MOF/NF, and Ru@NiCo–MOF/NF are shown in Fig. 2(a). For such four catalysts, the diffraction peaks at 2θ values of 44.54°, 51.9°, and 76.42° correspond to (1 1 1), (2 0 0), and (2 2 0) crystal planes of Ni (JCPDS No. 87-0712), respectively [30–33]. Due to the strong signal of the NF substrate along with the small diameter and low loading amount of NPs for metal such as Ru, there are no obvious characteristic peaks, consistent with findings reported in most previous studies.

X-ray photoelectron spectroscopy (XPS) results reflect the compositions of materials and valence states of various elements. The XPS survey spectrum in Fig. 2(b) is consistent with results of the element distribution, also indicating that there are four elements in Ru@NiFe–MOF/NF, i.e., Ru, Ni, Fe, and O, which aligns well with results of the EDS analysis. To further investigate the chemical bonding states of Ru, Ni, Fe, and O, we analyzed Ru@NiFe–MOF/NF based on high-resolution XPS spectra. As shown by the Fe 2p XPS spectrum in Fig. 2(c), two characteristic peaks appear near 713.2 and 723.0 eV, corresponding to Fe $2p_{3/2}$ and Fe $2p_{1/2}$, respectively [34–35], indicating the presence of both Fe^{3+} and Fe^{2+} in the catalyst. In Fig. 2(d), it is observed from the Ru 3p spectrum that there are Ru $3p_{3/2}$ and Ru $3p_{1/2}$ peaks at 463.2 and 485.4 eV, respectively, which are attributed to the presence of metallic Ru [36–38]. Peaks at 465.5 and 487.6 eV can be ascribed to the Ru−O bond, indicating that Ru NPs can be stably anchored to the ligand framework through the formation of interfacial bonds between the edge of Ru NPs and the carboxyl oxygen of NiFe–MOFs, which will significantly enhance the long-term catalytic stability. Ru^{n+} peaks with binding

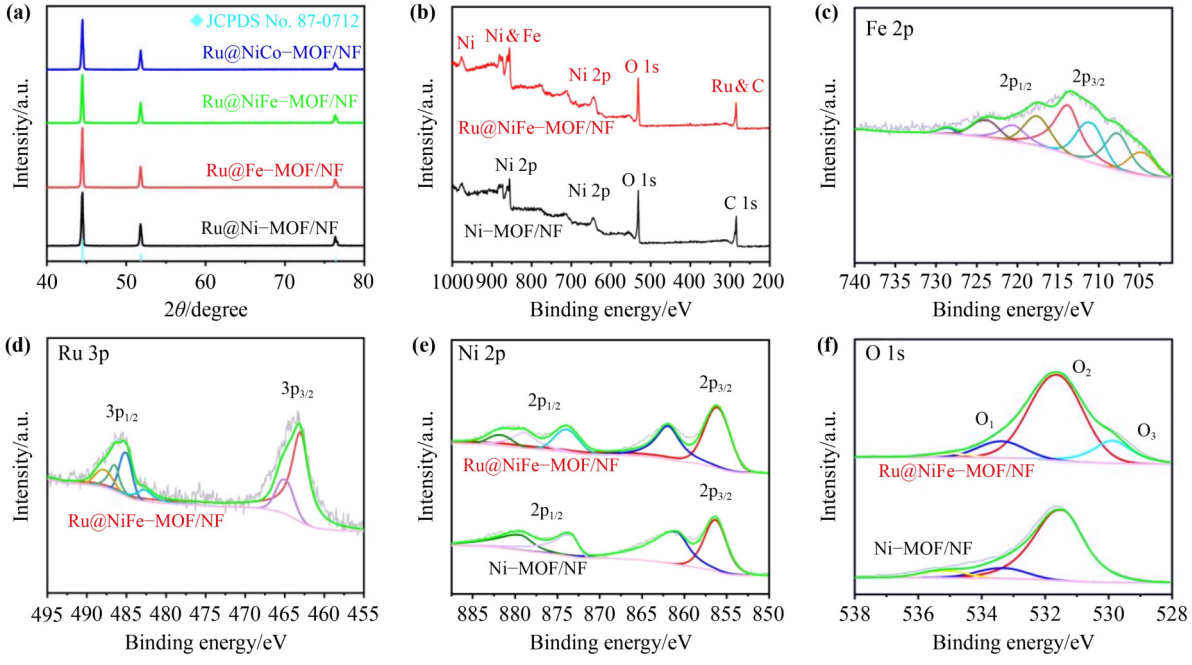

Fig. 2 (**a**) XRD patterns of catalysts. (**b**) XPS survey spectra of Ni–MOF/NF and Ru@NiFe–MOF/NF. (**c**) High-resolution Fe 2p XPS spectrum of Ru@NiFe–MOF/NF. (**d**) High-resolution Ru 3p XPS spectrum of Ru@NiFe–MOF/NF. (**e**)(**f**) High-resolution Ni 2p and O 1s XPS spectra of both Ni–MOF/NF and Ru@NiFe–MOF/NF.

energies located at 483.6 and 488.4 eV may be formed due to the surface oxidation of the catalyst when it is exposed to air. In the Ni 2p XPS spectrum shown in Fig. 2(e), two strong peaks at 873.4 and 855.5 eV correspond to Ni $2p_{1/2}$ and Ni $2p_{3/2}$, respectively, indicating the presence of Ni^{2+} in Ru@NiFe–MOF/NF. Meanwhile, other two peaks at 852.7 and 870.1 eV are attributed to metallic Ni 2p of the NF substrate [39–42]. Surprisingly, the O 1s spectrum shows a typical characteristic peak of Ru−O at 530.9 eV, as shown in Fig. 2(f), which indicates the formation of the Ru−O bond. The elemental contents of C, O, Fe, Ni, and Ru in the Ru@NiFe–MOF/NF catalyst based on XPS analysis are also revealed in Table S2 (included by ESM of Appendix).

By using inductively coupled plasma-atomic emission spectrometry (ICP-OES), the mass loadings of Ru on Ru@NiFe–MOF/NF were calculated to be about 0.03 wt.% when considering the entire electrode (Table S3 included by ESM of Appendix).

Figure 3(a) presents OER 95% *IR*-compensated linear sweep voltammetry (LSV) curves of Ru@Ni–MOF/NF, Ru@Fe–MOF/NF, Ru@NiFe–MOF/NF, Ru@NiCo–MOF/NF, Ni–MOF/NF, and RuO_2/NF. Among them, the target catalyst, Ru@NiFe–MOF/NF, exhibited the best OER performance. At a current density of 10 mA·cm^{-2}, its overpotential was 240 mV, which was lower than those of Ru@Fe–MOF/NF (260 mV), Ru@Ni–MOF/NF (270 mV), Ru@NiCo–MOF/NF (280 mV), Ni–MOF/NF (310 mV), and RuO_2/NF (250 mV). In addition, the overpotential of Ru@NiFe–MOF/NF was 280 mV at a current density of 50 mA·cm^{-2} while 320 mV at 100 mA·cm^{-2}. For comparison, representative of state-of-the-art Ru-based and transition metal-based OER electrocatalysts reported in the last three years, with overpotentials below 350 mV at 10 mA·cm^{-2} in 1 mol·L^{-1} KOH, are selected, as shown in Table 1 [43–52]. It is detected that the resulting Ru@NiFe–MOF/NF in this work has superior catalytic performance.

In addition, the Tafel slope of each catalyst was calculated to investigate the reaction kinetics. As shown in Fig. 3(b), the Tafel slope of Ru@NiFe–MOF/NF is 43 mV·dec^{-1}, which is lower than those of Ru@Fe–MOF/NF (44 mV·dec^{-1}), Ru@Ni–MOF/NF (79 mV·dec^{-1}), Ru@NiCo–MOF/NF (81 mV·dec^{-1}), Ni–MOF/NF (85 mV·dec^{-1}), and RuO_2/NF (281 mV·dec^{-1}), indicating that Ru@NiFe–MOF/NF has the best OER catalytic activity in this work.

The overpotentials of Ru@Ni–MOF/NF, Ru@Fe–MOF/NF, Ru@NiFe–MOF/NF, and Ru@NiCo–MOF/NF

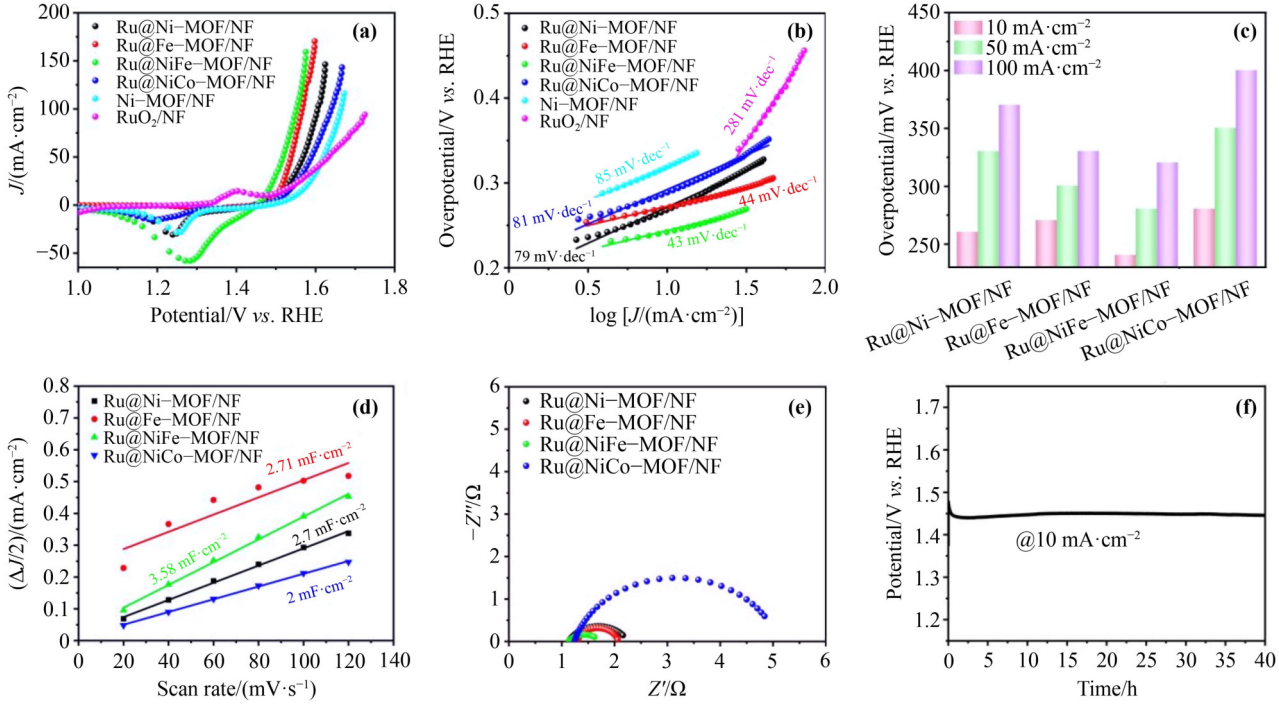

Fig. 3 (**a**) Polarization curves of different catalysts for OER. (**b**) Tafel slopes of obtained catalysts for OER. (**c**) Comparison of overpotentials for different catalysts at different current densities. (**d**) C_{dl} plots of the obtained catalyst. (**e**) Nyquist plots. (**f**) Chronopotentiometry tests of Ru@NiFe–MOF/NF at 10 mA·cm^{-2}.

Table 1 Comparison of OER performances between the Ru@NiFe–MOF/NF catalyst and other reported OER electrocatalysts in 1.0 mol·L^{-1} KOH

Catalyst	η_{10}/mV [a)]	Ref.
Ru@NiFe–MOF/NF	240	This work
$Ru_xFe_2Ni_5$	235	[43]
RuO_2/CoFe-LDH/NF	270	[44]
P–Ru–CoFe LDH	275	[45]
P–RuO_2	310	[46]
Ru–CoO	340	[47]
Ru SS/FeNiPi	204	[48]
def-Ru–NiFe LDH/NCO	225	[49]
$(Ru_2Fe_2Co_6)OOH$	248	[50]
Ru-SAC/NiFe LDH	196	[51]
Co/NFCH-FF	201	[52]

a) η_{10} is the overpotential at the current density of 10 mA·cm^{-2}, reflecting the OER activity.

at different current densities are shown in Fig. 3(c).

To further elucidate effective active sites on the catalyst surface, we performed a detailed investigation on catalysts using cyclic voltammetry (CV) at the scan rate ranging from 20 to 120 mV·s^{-1}, and the results are revealed in Figs. S8–S11 (included by ESM of Appendix). We also estimated the double-layer capacitance (C_{dl}) values of catalysts. The C_{dl} is usually employed as an indicator to evaluate the electrochemical active surface area (ECSA) of a catalyst [53]. As depicted in Fig. 3(d), the C_{dl} value of Ru@NiFe–MOF/NF is 3.58 mF·cm^{-2}, which is higher than those of Ru@Fe–MOF/NF (2.71 mF·cm^{-2}), Ru@Ni–MOF/NF (2.70 mF·cm^{-2}), and Ru@NiCo–MOF/NF (2 mF·cm^{-2}). It is widely recognized that the ECSA is directly proportional to the C_{dl}. For a catalyst, a higher C_{dl} implies a larger ECSA and a bigger number of active sites exposed on the interface, thereby promoting the enhancement of OER.

To gain a deeper understanding of the catalytic activity of Ru@NiFe–MOF/NF, electrochemical impedance spectroscopy (EIS) was conducted to further analyze the charge transfer resistance (R_{ct}) between the catalyst and electrolyte. As shown in Fig. 3(e), Ru@NiFe–MOF/NF has the smallest R_{ct}, meaning that it has the fastest catalytic reaction kinetics. This may be due to its excellent electrical conductivity, synergistic electronic coupling effect among different metal elements, and 3D highly open hierarchical porous structure, which help Ru@NiFe–MOF/NF effectively achieve rapid charge transfer [54–56].

Electrocatalysts are required to maintain good stability during practical applications. Thus we studied the electrochemical long-term stability of Ru@NiFe–MOF/NF for the OER process in 1 mol·L^{-1} KOH electrolyte using chronopotentiometry (CP). As shown in Fig. 3(f), there was no significant change in the voltage of Ru@NiFe–MOF/NF when it worked for 40 h at a current density of 10 mA·cm^{-2}, demonstrating its high stability for the OER process.

Similarly, we investigated HER performances of different samples in 1 mol·L^{-1} KOH solution and conducted electrochemical tests in a three-electrode system. Figure 4(a) presents LSV curves of Ru@Ni–MOF/NF, Ru@Fe–MOF/NF, Ru@NiFe–MOF/NF, Ru@NiCo–MOF/NF, Ni–MOF/NF, and Pt/C/NF. It is detected that among them, the target catalyst, Ru@NiFe–MOF/NF, exhibited the best HER performance. At a current density of 10 mA·cm^{-2}, its overpotential was 84 mV, obviously lower than those of Ru@Fe–MOF/NF (102 mV), Ru@Ni–MOF/NF (195 mV), Ru@NiCo–MOF/NF (226 mV), Ni–MOF/NF (293 mV), and Pt/C/NF (137 mV). In addition, the overpotential of Ru@NiFe–MOF/NF was 163 mV at a current density of 50 mA·cm^{-2} while 214 mV at 100 mA·cm^{-2}. The comparison results show that the catalytic performance of the Ru@NiFe–MOF/NF catalyst is superior to those of many reported Ru-based and transition metal-based HER catalysts. As shown in Table 2 [24,47,57–64], the selected catalysts are typical representatives of state-of-the-art Ru-based and transition metal-based electrocatalysts for HER reported in the last few years.

As is known to all, reaction kinetics can provide important basis for understanding HER pathways on electrocatalysts. As shown in Fig. 4(b), the Tafel slope of Ru@NiFe–MOF/NF is 95 mV·dec^{-1}, which is lower than those of Ru@Fe–MOF/NF (125 mV·dec^{-1}), Ru@Ni–MOF/NF (115 mV·dec^{-1}), Ru@NiCo–MOF/NF (96 mV·dec^{-1}), Ni–MOF/NF (108 mV·dec^{-1}), and Pt/C/NF (140 mV·dec^{-1}).

The overpotentials of Ru@Ni–MOF/NF, Ru@Fe–MOF/NF, Ru@NiFe–MOF/NF, and Ru@NiCo–MOF/NF at different current densities are also presented in Fig. 4(c).

Long-term durability is another important parameter for the practical application of catalysts. As shown in Fig. 4(d), Ru@NiFe–MOF/NF underwent long-term electrocatalytic HER testing at a constant current density

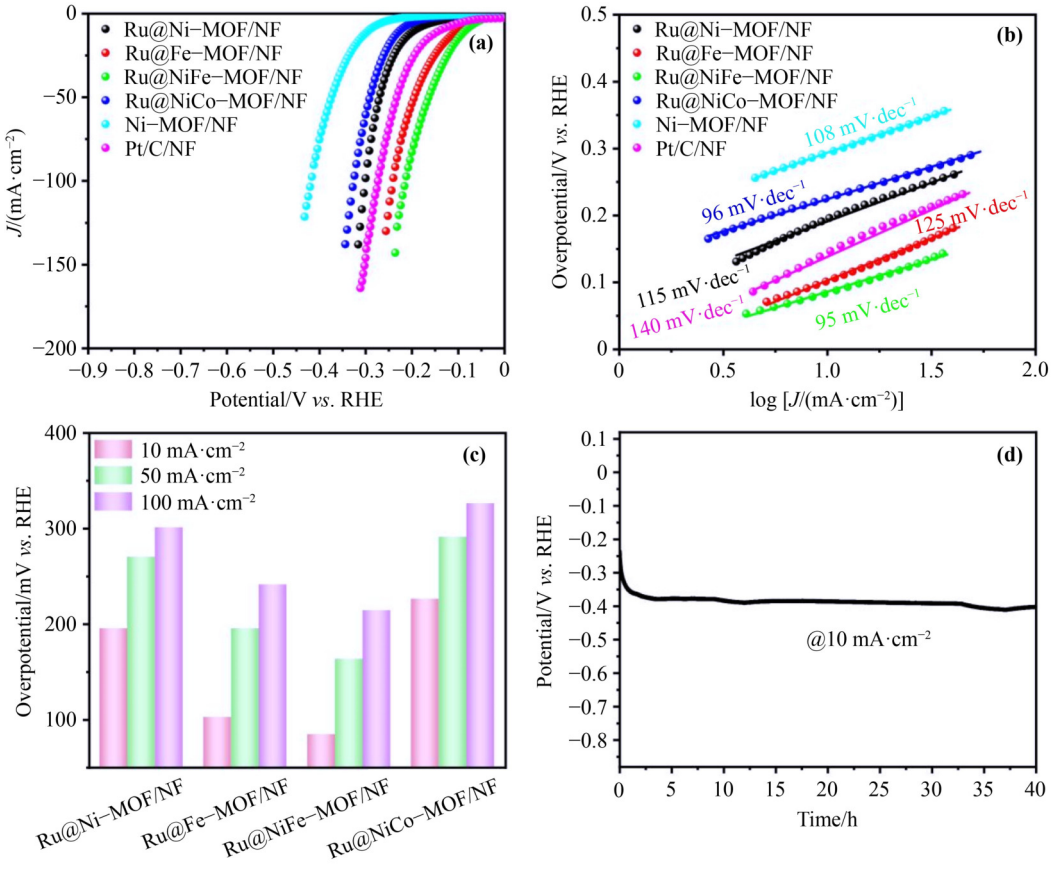

Fig. 4 (**a**) Polarization curves of different catalysts for HER. (**b**) Tafel slope of obtained catalysts for HER. (**c**) Comparison of overpotentials at different current densities of different catalysts. (**d**) CP test result of Ru@NiFe–MOF/NF at 10 mA·cm^{-2}.

Table 2 Comparison of HER performances between the Ru@NiFe–MOF/NF catalyst and other reported HER electrocatalysts in 1.0 mol·L^{-1} KOH

Catalyst	η'_{10}/mV [a]	Ref.
Ru@NiFe–MOF/NF	84	This Work
Ru–CoO	359	[47]
CoWCP-NPC-1:1	217	[57]
NiFeP/NCH	216	[58]
Ru–CoO@SNG	90	[59]
Ru–MoO_2@PC/rGO	126	[60]
RCFP/NF	112	[61]
FeCoSG/NCNT@Ru	21.1	[24]
CoRuP	12.9	[62]
Ru@HMCS/Ru–CoP	2.9	[63]
Ru_1Ni_6/CNF	14	[64]

a) η'_{10} is the overpotential at the current density of 10 mA·cm^{-2}, reflecting the HER activity.

of 10 mA·cm^{-2}. The CP curve was recorded over 40 h, with no significant change in the voltage during the testing process, indicating that Ru@NiFe–MOF/NF has excellent stability during the HER process.

4 Conclusion

In summary, the Ru@NiFe–MOF/NF catalyst has been prepared using a straightforward one-step hydrothermal method followed by thermal annealing. The synergistic interaction between Ru NPs and NiFe–MOFs endows Ru@Ni–MOF/NF with excellent catalytic performance. In 1 mol·L^{-1} KOH, the OER only requires an overpotential of 240 mV to reach a current density of 10 mA·cm^{-2}, while the HER needs 84 mV to reach 10 mA·cm^{-2}. Meanwhile, this catalyst also exhibits excellent long-term durability. Whether it is for OER or HER, Ru@NiFe–MOF/NF can work stably for 40 h at a current density of 10 mA·cm^{-2} without significant voltage fluctuations. Its excellent electrochemical performance can be attributed to three key factors. Firstly, the 3D NS structure effectively facilitates the mitigation of the NP agglomeration and promotes the penetration and transport of the electrolyte. Secondly, the valence states of Ru, Ni, and Fe are diverse, providing sufficient active sites for redox reactions and improving the electrical conductivity

of the material. Moreover, Fe^{3+} is also an effective promoter for the electrochemical OER catalytic reaction. Thirdly, the large specific surface area of the electrode material can provide more open channels and increase the accessibility of active sites, thereby enhancing the overall electrochemical performance of the material. This study not only provides a new type of alkaline water electrolysis catalyst with excellent catalytic performance, but also opens a new avenue for the rational design of other catalysts.

Declaration of competing interests The authors declare that they have no conflict of interests.

Acknowledgements This work was financially supported by the National Natural Science Foundation of China (Grant Nos. 52173257 and 52372064), the Major Research Program of Jingdezhen Ceramic Industry (Grant No. 2023ZDGG001), the Natural Science Foundation of Jiangxi Province (Grant Nos. 20232ACB204011 and 20224BAB204001), and the Opening Project of State Key Laboratory of New Ceramic Materials Tsinghua University (Grant Nos. KF202309 and KF202414).

Data availability statement Data presented in this study are available on request from corresponding authors.

Online appendix Electronic supplementary material (ESM) can be found in the online version at https://doi.org/10.1007/s11706-025-0731-2 and https://journal.hep.com.cn/foms/EN/10.1007/s11706-025-0731-2 that includes Figs. S1–S11 and Table S1–S3.

References

[1] Sun Y M, Xue Z Q, Liu Q L, et al. Modulating electronic structure of metal–organic frameworks by introducing atomically dispersed Ru for efficient hydrogen evolution. Nature Communications, 2021, 12(1): 1369

[2] Li W, Guo B, Zhang K, et al. Ru-regulated electronic structure CoNi–MOF nanosheets advance water electrolysis kinetics in alkaline and seawater media. Journal of Colloid and Interface Science, 2024, 668: 181−189

[3] Liu X, Zhang X, Liu R, et al. A Ni-doped Mn–MOF decorated on Ni-foam as an electrode for high-performance supercapacitors. Journal of Nanoparticle Research, 2022, 24(2): 23

[4] Pan C, Liu Z, Huang M. 2D iron-doped nickel MOF nanosheets grown on nickel foam for highly efficient oxygen evolution reaction. Applied Surface Science, 2020, 529: 147201

[5] Amirabad T N, Ensafi A A, Mousaabadi K Z, et al. Binder-free engineering design of Ni–MOF ultrathin sheet-like grown on PANI@GO decorated nickel foam as an electrode for in hydrogen evolution reaction and asymmetric supercapacitor. International Journal of Hydrogen Energy, 2023, 48(76): 29471−29484

[6] Chen C, Jin L, Dong H, et al. Modulating adsorption of active hydrogen atoms on palladium nanoparticles: doping ruthenium into metal–organic frameworks for efficient electrocatalytic hydrodechlorination. Separation and Purification Technology, 2023, 324: 124527

[7] Dai Z, Du X, Zhang X. Controlled synthesis of $NiCo_2O_4$@Ni–MOF on Ni foam as efficient electrocatalyst for urea oxidation reaction and oxygen evolution reaction. International Journal of Hydrogen Energy, 2022, 47(39): 17252−17262

[8] Ebrahimi-Koodehi S, Ghodsi F E, Mazloom J. Ni/Mn metal–organic framework decorated bacterial cellulose (Ni/Mn–MOF@BC) and nickel foam (Ni/Mn–MOF@NF) as a visible-light photocatalyst and supercapacitive electrode. Scientific Reports, 2023, 13(1): 19260

[9] Feng C, An Q, Zhang Q, et al. Unleashing the potential of Ru/FeCo–MOF in water splitting and supercapacitors through morphology and electronic structure control. International Journal of Hydrogen Energy, 2024, 55: 189−198

[10] Guo G. Direct fabrication of mixed metal–organic frameworks (Ni/Cu–MOF) and C@$NiCu_2O_4$ onto Ni foam as binder-free high performance electrode for supercapacitors. Journal of Materials Science: Materials in Electronics, 2021, 32(12): 16287−16301

[11] He N, Chen X, Fang B, et al. Zr–MOF/NiS_2 hybrids on nickel foam as advanced electrocatalysts for efficient hydrogen evolution. Journal of Colloid and Interface Science, 2023, 640: 820−828

[12] Hu Z P, Geng Q, Dong S J, et al. MOF-derived low Ru-loaded high entropy alloy as an efficient and durable self-supporting electrode in rechargeable liquid/flexible Zn–air batteries. Journal of Colloid and Interface Science, 2024, 671: 34−45

[13] Huang S, Shi X R, Sun C, et al. Template-controlled *in-situ* growing of NiCo–MOF nanosheets on Ni foam with mixed linkers for high performance asymmetric supercapacitors. Applied Surface Science, 2022, 572: 151344

[14] Jabarian S, Ghaffarinejad A. Electrochemical synthesis of NiBTC metal organic framework thin layer on nickel foam: an efficient electrocatalyst for the hydrogen evolution reaction. Journal of Inorganic and Organometallic Polymers and Materials, 2019, 29(5): 1565−1574

[15] Jia H, Lu S, Ra Shin S H, et al. *In situ* anodic electrodeposition of two-dimensional conductive metal–organic framework@ nickel foam for high-performance flexible supercapacitor. Journal of Power Sources, 2022, 526: 231163

[16] Jing L, Wang Y, Jiang W, et al. Ruthenium-doped bimetallic organic framework self-supported electrodes as efficient electrocatalysts for oxygen evolution reaction. International Journal of Hydrogen Energy, 2024, 69: 195−202

[17] Li Y, He N, Chen X, et al. Interface regulation of Zr–MOF/Ni_2P@nickel foam as high-efficient electrocatalyst for pH-universal hydrogen evolution reaction. Journal of Colloid and Interface Science, 2024, 656: 289−296

[18] Lin Y, Zhang M, Zhao L, et al. Ru doped bimetallic phosphide derived from 2D metal organic framework as active and robust electrocatalyst for water splitting. Applied Surface Science, 2021, 536: 147952

[19] Ling Q, Yan K, Zhao Z, et al. Oxygen-vacancy-rich Ru nanoclusters doped NiCo metal–organic framework for driving overall water electrolysis and supercapacitors. Journal of Power Sources, 2024, 613: 234851

[20] Ling X, Du F, Zhang Y, et al. Preparation of an Fe_2Ni MOF on nickel foam as an efficient and stable electrocatalyst for the oxygen evolution reaction. RSC Advances, 2019, 9(57): 33558−33562

[21] Salehi S, Ehsani M H, Aghazadeh M, et al. Electrodeposition of binderless Ni,Zn–MOF on porous nickel substrate for high-efficiency supercapacitors. Journal of Solid State Chemistry, 2022, 316: 123549

[22] Salman M, Qin H, Zou Y, et al. *In-situ* decoration of NiCo-thiophene based metal–organic framework on nickel foam as an efficient electrocatalyst for oxygen evolution reaction. Journal of Power Sources, 2025, 629: 235942

[23] Zhu M, Cai W, Wang H, et al. Rational construction of MOF-derived Zn–Co–O/NiCo-LDH core/shell nanosheet arrays on nickel foam for high-performance supercapacitors. Journal of Alloys and Compounds, 2021, 884: 160931

[24] Zheng H, Jiang Z J, Jiang Z. CoFe embedded in nitrogen-doped porous carbon with spider-egg structure derived from MOFs promote the dispersion of Ru nanoparticles for high-performance hydrogen-evolution-reaction. International Journal of Hydrogen Energy, 2024, 51: 193−205

[25] Zhi G, Qi X, Li Y, et al. Efficient treatment of smelting wastewater: 3D nickel foam@MOF shatters the previous limitation, enabling high-throughput selective capture of arsenic to form non-homogeneous nuclei. Separation and Purification Technology, 2024, 328: 124927

[26] Liu C, Tseng C Y, Wang Y C, et al. Low-pressure plasma-processed ruthenium/nickel foam electrocatalysts for hydrogen evolution reaction. Materials, 2022, 15(7): 2603

[27] Lu M, Sun J, Cui B, et al. Construction of Pd, Ru/2D MXene nanosheets/3D self-supporting nickel foam composite electrode and its electrocatalytic synergistic degradation of antibiotics. Separation and Purification Technology, 2024, 340: 126736

[28] Miao F J, Lu Y, Tao B R, et al. Nickel foam-loaded Co–MOF@TiO_2/MoS_2 as electrode materials for dual-function devices for glucose detection and hydrogen evolution. Mikrochimica Acta, 2024, 191(8): 469

[29] Xiao X, Wang X, Jiang X, et al. *In situ* growth of Ru nanoparticles on $(Fe,Ni)(OH)_2$ to boost hydrogen evolution activity at high current density in alkaline media. Small Methods, 2020, 4(6): 1900796

[30] Qu H, Ma Y, Gou Z, et al. Ni_2P/C nanosheets derived from oriented growth Ni–MOF on nickel foam for enhanced electrocatalytic hydrogen evolution. Journal of Colloid and Interface Science, 2020, 572: 83−90

[31] Wang F, Li Y, Xie H, et al. Pd nanoparticles supported on microflower NiMOF modified roughed nickel foam with the enhanced active site for electrochemical dechlorination of trichloroacetic acid. Separation and Purification Technology, 2023, 325: 124598

[32] Wang H, Zhang Y, Wu G, et al. Ru nanoparticles decorating ferrocene-based metal–organic framework for efficient and stable water-splitting electrocatalyst. International Journal of Hydrogen Energy, 2024, 64: 261−268

[33] Wang H, Zou H, Liu Y, et al. Ni_2P nanocrystals embedded Ni–MOF nanosheets supported on nickel foam as bifunctional electrocatalyst for urea electrolysis. Scientific Reports, 2021, 11(1): 21414

[34] Weng S, An Q, Xu Y, et al. *In-situ* formation of NiFe–MOF on nickel foam as a self-supporting electrode for flexible electrochemical sensing and energy conversion. Chemosensors, 2023, 11(4): 242

[35] Zhang X, Yin Q, Cao F, et al. Synthesis of NiFe–MOF@NiFeTe nanoparticle-rod heterostructure on nickel foam for high-performance hybrid supercapacitors. Applied Surface Science, 2023, 616: 156533

[36] Xu J, Yu L, Dong B, et al. Ruthenium–nickel oxide derived from Ru-coupled Ni metal–organic framework for effective oxygen evolution reaction. Journal of Colloid and Interface Science, 2024, 654: 1080−1088

[37] Yang S, Yu J, Jiang T, et al. High performance symmetric solid state supercapacitor based on electrode of $Ru_xNi_{1-x}Co_2O_4$ grown on nickel foam. Journal of Alloys and Compounds, 2018, 764: 767−775

[38] Zhao P, Liu Q, Yang X, et al. Ru nanocrystals modified porous FeOOH nanostructures with open 3D interconnected architecture supported on NiFe foam as high-performance electrocatalyst for oxygen evolution reaction and electrocatalytic urea oxidation.

Journal of Colloid and Interface Science, 2024, 673: 49−59

[39] Ravipati M, Badhulika S. Solvothermal synthesis of hybrid nanoarchitectonics nickel–metal organic framework modified nickel foam as a bifunctional electrocatalyst for direct urea and nitrate fuel cell. Advanced Powder Technology, 2023, 34(8): 104087

[40] Ren T, Wang J, Yu X H, et al. The electrocatalytic self-reconstruction of ultrathin 2D MOF nanoarrays supported on alloy foam improves the oxygen evolution reaction. Colloids and Surfaces A: Physicochemical and Engineering Aspects, 2024, 684: 133136

[41] Senthil Raja D, Lin H W, Lu S Y. Synergistically well-mixed MOFs grown on nickel foam as highly efficient durable bifunctional electrocatalysts for overall water splitting at high current densities. Nano Energy, 2019, 57: 1−13

[42] Wu C F, Chung R J, Kongvarhodom C, et al. *In-situ* grown nickel iron bimetal organic frameworks from activated Ni foam for efficient energy storage and electrocatalysis: study of metal ratio and nickel precursor effects. Journal of Power Sources, 2024, 594: 233968

[43] Chen J, Li T, Zhong S, et al. Ruthenium-doped $FeNi_3$@nickel–iron hydroxide nanoparticles aerogel for highly efficient oxygen evolution reaction. International Journal of Hydrogen Energy, 2025, 106: 216−225

[44] Chen Q, Yu Y, Luo S, et al. Trace ruthenium dioxide stabilize active center of CoFe-LDH for efficient water electrolysis. International Journal of Hydrogen Energy, 2024, 84: 401−409

[45] Li J, Shi J, Hu Y, et al. Plasma-induced vacancy defects of Ru-doped CoFe layered double hydroxide for superior oxygen evolution activity. Journal of Alloys and Compounds, 2024, 976: 173076

[46] Qiu T, Liang Z, Guo W, et al. Highly exposed ruthenium-based electrocatalysts from bimetallic metal–organic frameworks for overall water splitting. Nano Energy, 2019, 58: 1−10

[47] Wu H W, Cui Y, Gao G H, et al. Atomic Ru-modulated Ru–CoO heterostructures as efficient bifunctional electrocatalyst for oxygen and hydrogen evolution reactions. Journal of Alloys and Compounds, 2023, 960: 170847

[48] Lu S Y, Huang B L, Sun M Z, et al. Synthetic tuning stabilizes a high-valence Ru single site for efficient electrolysis. Nature Synthesis, 2024, 3: 576−585

[49] Dao H T, Hoa V H, Sidra S, et al. Dual efficiency enhancement in overall water splitting with defect-rich and Ru atom-doped NiFe LDH nanosheets on $NiCo_2O_4$ nanowires. Chemical Engineering Journal, 2024, 485: 150054

[50] Zhu Y, Zhang S Q, Chen R Z, et al. Controllable electronic transfer tailoring d-band center via cobalt-oxygen-bridged Ru/Fe dual-sites for boosted oxygen evolution. Small, 2024, 20(25): 2310611

[51] Israr M, Ali S, Zhang J, et al. NiFe LDH hollow nanocages confined Ru single atoms for remarkable oxygen evolution reaction. Small, 2025, 5: 2500828

[52] Yu L, Chen H H, Ma G Y, et al. Co-doped NiFe carbonate hydroxide hydrate nanosheets with edge effect constructed from spent lithium-ion battery ternary cathodes for oxygen evolution reaction. Journal of Colloid and Interface Science, 2024, 668: 190−201

[53] Mohammadi T, Asadpour-Zeynali K, Majidi M R, et al. Ru–Ni nanoparticles electrodeposited on rGO/Ni foam as a binder-free, stable and high-performance anode catalyst for direct hydrazine fuel cell. Heliyon, 2023, 9(6): e16888

[54] Palanisamy S, Wu H M, Lee L Y, et al. Fabrication of 3D amino-functionalized metal–organic framework on porous nickel foam skeleton to combinate follicle stimulating hormone antibody for specific recognition of follicle-stimulating hormone. JACS Au, 2021, 1(12): 2249−2260

[55] Poimenidis I A, Lykaki M, Loukakos P A, et al. Ultra-high supercapacitor performance of NiSRu@NiO nanocomposites on nickel foam electrodes. Journal of Energy Storage, 2024, 83: 110679

[56] Tseng C Y, Cheng I C, Chen J Z. Low-pressure-plasma-processed NiFe–MOFs/nickel foam as an efficient electrocatalyst for oxygen evolution reaction. International Journal of Hydrogen Energy, 2022, 47(85): 35990−35998

[57] Zhang Y N, Shi W P, Bo L L, et al. Electrospinning construction of heterostructural Co_3W_3C/CoP nanoparticles embedded in N, P-doped hierarchically porous carbon fibers as excellent multifunctional electrocatalyst for Zn–air batteries and water splitting. Chemical Engineering Journal, 2022, 431: 134188

[58] Wei Y S, Zhang M, Kitta M, et al. A single-crystal open-capsule metal–organic framework. Journal of the American Chemical Society, 2019, 141(19): 7906−7916

[59] Naseeb W, Liu Q, Nichols F, et al. Ru–CoO heterostructured nanoparticles supported on nitrogen and sulfur codoped graphene nanosheets as effective electrocatalysts for hydrogen evolution reaction in alkaline media. Journal of Electroanalytical Chemistry, 2023, 932: 117272

[60] Han J Y, Cai S H, Zhu J Y, et al. MOF-derived ruthenium-doped amorphous molybdenum dioxide hybrid for highly efficient hydrogen evolution reaction in alkaline media. Chemical Communications, 2022, 58(1): 100−103

[61] Jang K, Yoon K, Hyoung J S, et al. Enhancement of hydrogen evolution activity by tailoring the electronic structure in ruthenium-heteroatom-doped cobalt iron phosphide nanoframes.

Applied Catalysis B: Environmental, 2024, 341: 123327

[62] El-Refaei S M, Russo P A, Schultz T, et al. Activating Ru in the pyramidal sites of Ru_2P-type structures with earth-abundant transition metals for achieving extremely high HER activity while minimizing noble metal content. Carbon Energy, 2024, 6(9): e556

[63] Du Y M, Zhan L, Li S S, et al. The unique core–shell structure drives the richness and high utilization of Ru species to stimulate the HER performance exceeding Pt. Fuel, 2024, 365: 131250

[64] Huang T T, Xiao J, Liu X, et al. Engineering Ru and Ni sites relay catalysis and strong metal-support interaction for synergetic enhanced electrocatalytic hydrogen evolution performance. Chemical Engineering Journal, 2025, 509: 161348